Superconducting properties of Bernevig-Hughes-Zhang model: Theory and applications to transition metal dichalcogenides

Haijiao Ji and Noah F. Q. Yuan*
Harbin Institute of Technology, Shenzhen 518055, People's Republic of China

(Received 6 November 2023; revised 15 January 2024; accepted 23 January 2024; published 14 February 2024)

We investigate the superconducting properties of two-dimensional topological materials, in particular the quantum spin Hall system with on-site pairing. Accordingly, three types of edge states are found, which are topologically protected fermionic states at zero field, topologically protected Majorana states at finite Zeeman fields, and unpaired fermionic states without topological protection. Applications to transition metal dichalcogenides are also discussed.

DOI: 10.1103/PhysRevB.109.054510

I. INTRODUCTION

Topology and superconductivity have been among the central topics of the condensed matter physics in recent decades. In particular, topological materials with nontrivial band topology would support topological states on the boundaries. Recently, several materials are found to host both topological band structure and superconductivity in experiments, such as doped Bi_2Se_3 [1–5], transition metal dichalcogenides [6–27], and iron-based superconductors [28–37]. As the combination of topology and superconductivity, topological superconductivity has been proposed to host the Majorana zero-energy modes (MZMs) [38–42], which are believed to have potential applications in topological quantum computation [43–45]. As a result, intensive studies on the superconducting phase of topological materials have been carried out in the recent decade in hope of searching for topological superconductivity.

In three dimensions, Fu and Kane proposed that the superconducting surface of a topological insulator could host MZMs within the vortices [41]. As one of the possible platforms, bulk iron-based superconductors were theoretically [46] predicted and experimentally [31,33] found to host topological surface states and hence topological superconductivity would be expected in such materials.

In two dimensions, Qi, Hughes, and Zhang [47] studied the superconducting phase of a quantum anomalous Hall system [48] whose time-reversal symmetry is spontaneously broken, and Majorana chiral edge states were predicted. Moreover, Wang, Xu, and Zhang [49] analyzed the superconducting phases of a quantum spin Hall (QSH) system [50–52] whose time-reversal symmetry is respected, and superconductivity can be realized intrinsically. Experimentally the monolayer iron-based superconductor was also found to host QSH edge states [35], and theoretically higher order topological superconductivity with Majorana corner states was predicted under certain circumstances [53–55].

In this work, we focus on the monolayer transition metal dichacogenides (TMDs) such as 4Hb-TaS_2 [26,27], 2*M*-WS_2 [18–22], 1T'-MTe_2 and T_d-MTe_2 (M = Mo and W). In these materials, all have been found intrinsically superconducting, 2*M*-WS_2, 1T'-MTe_2 and T_d-MTe_2 are found to host QSH edge states, and 4Hb-TaS_2 could be regarded as a QSH system in the topologically trivial phase. As a result, the general results of Wang, Xu, and Zhang could apply. However, as the TMDs in general have lower symmetries, some conclusions due to accidental degeneracy need to be modified. Furthermore, the roles of external electromagnetic fields are also discussed in our manuscript. Under an external out-of-plane electric field, the accidental degeneracy between some pairings are lifted, and some pairings are allowed to mix. Under an external in-plane magnetic field, Majorana flat bands or Majorana chiral edge states will in general emerge as long as the pairing symmetry is not the conventional *s* wave. However, we point out that unpaired QSH edge states may also coexist with Majorana edge states when the pairing symmetry is not the conventional *s* wave.

II. SYMMETRY CLASSIFICATION OF PAIRINGS

It is known that the Bernevig-Hughes-Zhang (BHZ) model [51] could describe the low-energy band structure of QSH states. We consider the BHZ model with pairing potential, whose Bogouliubov–de Gennes (BdG) Hamiltonian at momentum $\mathbf{k}$ reads

$$H_{\mathrm{BdG}}(\mathbf{k}) = \begin{pmatrix} H_{\mathrm{BHZ}}(\mathbf{k}) - \mu & H_{\Delta}(\mathbf{k}) \\ H_{\Delta}^{\dagger}(\mathbf{k}) & -H_{\mathrm{BHZ}}^{*}(-\mathbf{k}) + \mu \end{pmatrix}, \quad (1)$$

where chemical potential is μ, the BHZ Hamiltonian is

$$H_{\mathrm{BHZ}}(\mathbf{k}) = \mathcal{A}(\tau_x\sigma_z k_y - \tau_y k_x) + (\mathcal{M} - \mathcal{B}k^2)\tau_z, \quad (2)$$

with the Pauli matrices σ_i and τ_i in the spin and orbital space respectively, and H_{Δ} is the pairing term.

Due to the particle-hole redundancy,

$$H_{\Delta}^{\mathrm{T}}(-\mathbf{k}) = -H_{\Delta}(\mathbf{k}). \quad (3)$$

*fyuanaa@connect.ust.hk

TABLE I. Classification of two-orbital pairing potentials. $\Delta_{\text{bulk}}(\mathbf{k})$ and $\Delta_{\text{edge}}(\mathbf{t})$ are effective pairing of bulk and QSH edge states via projecting the BdG Hamiltonian into the conduction band. $\Delta_{\text{edge}}(\mathbf{t})$ depends on the tangential unit vector $\mathbf{t}$ along the edge state propagating direction. Pauli matrices σ_i and τ_i are in the spin and orbital space respectively.

	H_Δ	$\Delta_{\text{bulk}}(\mathbf{k})$	$\Delta_{\text{edge}}(\mathbf{t})$	$D_{\infty h}$	C_{2h}	C_{2v}	C_{3v}
Δ_0	$i\tau_0\sigma_y$	σ_0	σ_0	A_{1g}	A_g		
Δ_z	$i\tau_z\sigma_y$	$(\mathcal{M}-\mathcal{B}k^2)\sigma_0/\mu$	0			A_1	A_1
Δ_1	$i\tau_y\sigma_0$	$\mathcal{A}(\mathbf{k}\times\boldsymbol{\sigma})_z/\mu$	0	A_{1u}	A_u		
Δ_2	$\tau_y\sigma_z$	$\mathcal{A}(\mathbf{k}\times\boldsymbol{\sigma})/\mu$	0	A_{2u}	B_u	A_2	A_2
Δ_x	$i\tau_x\sigma_y$	$-\mathcal{A}k_y\sigma_z/\mu$	$-t_y\sigma_z$	E_{1u}	A_u	B_1	E
Δ_y	$\tau_y\sigma_x$	$\mathcal{A}k_x\sigma_z/\mu$	$t_x\sigma_z$		B_u	B_2	

For on-site pairings, H_Δ is an antisymmetric 4 by 4 matrix, which can be expanded by 6 linearly independent matrices as listed in Table I, with corresponding coefficients $\Delta_{0,1,2}$ and $\Delta_{x,y,z}$. These six pairing matrices can be classified with respect to the symmetry group of the BHZ model.

The maximal symmetry group of the BHZ model in Eq. (2) is $D_{\infty h}\ltimes \mathrm{U}(1)$, where point group $D_{\infty h}$ has continuous in-plane rotation $C_z(\theta)=\exp(i\sigma_z\tau_z\theta/2)$, vertical mirror reflections $M_y=i\sigma_y$ and horizontal mirror reflection $M_z=i\sigma_z$, and the spin-U(1) rotation is $U(\phi)=\exp(M_z\phi/2)$. Notice that $D_{\infty h}$ and spin-U(1) do not commute due to the spin-orbit coupling (SOC). Under point group $D_{\infty h}$, $\Delta_{0,z}$ furnish the trivial representation A_{1g}, $\Delta_1(\Delta_2)$ furnishes $A_{1u}(A_{2u})$, and (Δ_x,Δ_y) furnish the two-dimensional (2D) representation E_{1u}.

In realistic crystals, the point group will be reduced to D_{nh} with integer $n=3,4,6$. The point group of monolayer $FeTe_{1-x}Se_x$ is D_{4h}, and superconductivity together with QSH has been found in experiments. Its low-energy band structure can be described by the BHZ model [28–30,35,53]. From experiments, the possible pairing of $FeTe_{1-x}Se_x$ may be $s_\pm$ wave, which could be realized by a mixture of Δ_0 and Δ_z pairings as elaborated in the next section. The point group of 2D 4Hb-TaS_2 is D_{6h}, and the unit cell of 4Hb-TaS_2 is formed by four monolayers, with two metalic and two insulating, where the low-energy physics of metalic layers can be described by the BHZ model but in the topologically trivial regime [24,25]. From experiments, the possible pairing of 4Hb-TaS_2 may be the time-reversal breaking chiral phase [26] or time-reversal invariant (TRI) nematic phase [27], which could be understood by the order parameter configuration of (Δ_x,Δ_y) pairing. We expand the free energy in terms of $\Delta_\pm\equiv\Delta_x\pm i\Delta_y$ up to the quartic order

$$f=\alpha(|\Delta_+|^2+|\Delta_-|^2)+\beta(|\Delta_+|^2+|\Delta_-|^2)^2 +\beta'|\Delta_+|^2|\Delta_-|^2. \tag{4}$$

When $\beta'>0$, f is minimized by the chiral pairing with either positive chirality $(\Delta_+,\Delta_-)=\Delta(1,0)$ or negative chirality $(\Delta_+,\Delta_-)=\Delta(0,1)$. When $\beta'<0$, f is minimized by the nematic pairing $(\Delta_x,\Delta_y)=\Delta(\cos\varphi,\sin\varphi)$, which is characterized by the nematic angle $\varphi\in[0,\pi)$. For point group $D_{\infty h}$, φ is continuous. For point group D_{6h}, φ takes discrete values $m\pi/3$ or $\pi/6+m\pi/3$ with integer $m=0,1,2$. The possible nematic angles of D_{3h} are the same as that of D_{6h}. For point group D_{4h}, $\varphi=m\pi/2$ or $\pi/4+m\pi/2$ with integer $m=0,1$.

It is interesting to note that, given the symmetry group $D_{nh}\ltimes \mathrm{U}(1)$ with $n=3,4,6,\infty$, the combination (Δ_1,Δ_2) furnish the 2D real representation of spin-U(1) group and hence $\Delta_{1,2}$ are degenerate. This degeneracy between Δ_1 and Δ_2 is protected by spin-U(1) symmetry, or equivalently mirror symmetry M_z. In the following we try to break the horizontal mirror symmetry M_z and consider pairings under such conditions.

In TMDs with low-symmetry structures, M_z can be broken by crystal fields. The point group of 2M-WS_2 and 1T'-MTe_2 is the same C_{2h}, including twofold rotation $C_{2y}=i\sigma_y\tau_z$ and inversion $I=\tau_z$. Since C_{2h} is Abelian, no 2D irreducible representations can be found, and the time-reversal symmetry will not be spontaneously broken. As a result, we find $\Delta_{0,z}$ belong to the trivial phase A_g, $\Delta_{1,x}$ to A_u and $\Delta_{2,y}$ to B_u. The point group of T_d-MTe_2 is C_{2v}, including mirror reflections $M_x=i\sigma_x\tau_z$, $M_y=i\sigma_y$ and twofold rotation $C_{2z}=i\sigma_z\tau_z$. Since C_{2v} is also Abelian, we find $\Delta_{0,1,z}$ belong to the trivial phase A_1, Δ_2 to A_2 and $\Delta_x(\Delta_y)$ to $B_1(B_2)$. Besides, M_z can also be broken by an external out-of-plane electric field, such as MoS_2 under ionic liquid gating, whose point group is C_{3v} and the possible pairings are $\Delta_{0,1,z}$ in the trivial phase A_1, Δ_2 in A_2 and (Δ_x,Δ_y) in E [25].

Besides breaking horizontal mirror symmetry M_z, one can also break the spin-U(1) symmetry by applying in-plane magnetic fields, which couple to electron spins along in-plane directions via the Zeeman effect. Before that, we first review the band structures and effective pairings for each pairing channel at zero field.

III. EFFECTIVE PAIRINGS AT ZERO MAGNETIC FIELD

At zero field, energy spectra with different s-wave pairings are plotted in Fig. 1 with open boundary conditions. In the Δ_0 pairing [Fig. 1(a)], both the bulk states and QSH edge states are fully gapped and topologically trivial, while the QSH edge states can stay unpaired in the Δ_z pairing [Fig. 1(b)]. In the chiral pairing $\Delta_\pm\equiv\Delta_x\pm i\Delta_y$ [Fig. 1(c)], the time-reversal symmetry (TRS) is spontaneously broken, and chiral edge states emerge under nonzero Chern number. At zero field, the Chern number is always even and the chiral edge states are fermionic [inset of Fig. 1(c)]. Δ_1 and Δ_2 share the same spectrum at zero field [Fig. 1(d)], with TRS-protected helical edge states with twofold degeneracy [inset of Fig. 1(d)]. The nematic pairing Δ_x [Figs. 1(e) and 1(f)] is nodal in the bulk and hosts fermionic flat bands on the edge at zero field. Such behaviors can be understood by effective pairings among states near chemical potential μ.

The effective pairing matrix $\Delta_{\text{bulk}}(\mathbf{k})$ among bulk eigenstates $\psi_{\mathbf{k}\uparrow,\downarrow}$ of the BHZ model in Eq. (2), is defined on the Nambu basis $(\psi_{\mathbf{k}\uparrow},\psi_{\mathbf{k}\downarrow})\Delta_{\text{bulk}}(\mathbf{k})(-\psi^\dagger_{-\mathbf{k}\downarrow},\psi^\dagger_{-\mathbf{k}\uparrow})^{\mathrm{T}}$. For different pairing channels $\Delta_{\text{bulk}}(\mathbf{k})$ are summarized in Table I. As shown in Figs. 1(c)–1(f) and Table I, at zero field, Δ_0 denotes the conventional s-wave pairing, Δ_z denotes the extended s-wave pairing, and the mixture of Δ_0 and Δ_z can describe $s_\pm$-wave pairing. Both Δ_1 and Δ_2 correspond to helical p-wave pairing but with different momentum-spin locking patterns,

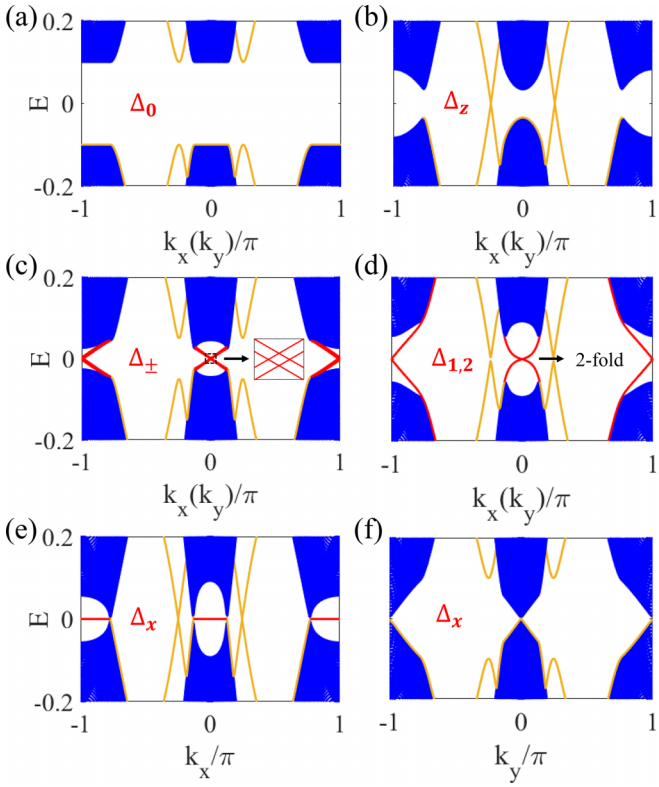

FIG. 1. BdG spectra at zero field. Blue regions denote bulk states, orange lines denote QSH edge states on the open boundary [(a), (c), (f) paired and (b), (d), (e) unpaired] and red lines denote topological edge states due to pairings [(c) chiral edge states, (d) helical edge states and (e) flat bands]. The model parameters are $(A, B, M_0, M_1, \mu, \Delta, a) = (1, 0, 0.5, 1, 0.7, 0.1, 1)$ in Eq. (5).

the nematic pairing $\Delta_x(\Delta_y)$ corresponds to $p_x(p_y)$-wave pairing, and the chiral pairing $\Delta_\pm \equiv \Delta_x \pm i\Delta_y$ corresponds to $(p \pm ip)$-wave pairing respectively.

When μ is low, QSH edge states will be involved in superconductivity, whose effective pairing $\Delta_{\text{edge}}(\mathbf{t})$ depends on the unit tangential vector $\mathbf{t}$ along the edge. As shown in Figs. 1(b), 1(d), 1(e) and Table I, at zero field, $\Delta_{1,2,z}$ would not induce pairings in QSH edge states along any direction, while nematic phase $(\Delta_x, \Delta_y) = \Delta(\cos\varphi, \sin\varphi)$ would not induce pairings in QSH edge states along the nematic direction $(\cos\varphi, \sin\varphi)$ only. Since the bulk states have orbital and spin degrees of freedom while the QSH edge states only have spin one, the existence of zero pairing channels for edge states should be general. The reasons for unpaired QSH edge states in Δ_z and nematic phase $(\Delta_x, \Delta_y) = \Delta(\cos\varphi, \sin\varphi)$ depend on the SOC details of the BHZ model. In general, due to Kramer's pairs along the same edge, the equal-spin pairings will not be allowed for QSH edge states, and $\Delta_{1,2}$ would not induce pairings in QSH edge states along any direction.

IV. TOPOLOGICAL SUPERCONDUCTIVITY UNDER IN-PLANE MAGNETIC FIELDS

Now we turn on the external in-plane magnetic field, which mainly couples to the spin via the Zeeman effect in 2D, and hence can be treated as a pure Zeeman field $\mathbf{B} = (B_x, B_y, 0)$ in the rest of this paper.

If $\mathcal{T}$ is spontaneously broken by the pairing such as the chiral pairing $(\Delta_x, \Delta_y) = \Delta(\pm i, 1)$ with point group D_{nh} or C_{nv} $(n = 3, 4, 6, \infty)$, under finite $\mathbf{B}$ the Chern number can become odd and Majorana chiral edge states will emerge as will be elaborated later.

If $\mathcal{T}$ and M_z are preserved by the pairing such as the nematic pairing $(\Delta_x, \Delta_y) = \Delta(\cos\varphi, \sin\varphi)$ with point group D_{nh} $(n = 3, 4, 6, \infty)$, under finite $\mathbf{B}$ the pseudo-time-reversal symmetry (PTRS) $\tilde{\mathcal{T}} \equiv \mathcal{T}\mathcal{M}_z$ is also respected. The pairing phase is hence in the BDI class [56–60], with particle-hole symmetry $\mathcal{P}$ and chiral symmetry $\mathcal{C} = \tilde{\mathcal{T}}\mathcal{P}$, which allows to define the topological charge for each bulk nodal point. With open boundary conditions, (Majorana) flat bands emerge between two nodal points with opposite net topological charges.

As long as $\mathcal{T}$ and the crystal symmetries are preserved by the pairing such as $\Delta_{1,2}$ and $\Delta_{x,y}$ pairings with point group D_{nh} $(n = 3, 4, 6, \infty)$ or C_{2h}, PTRS can also be found $\tilde{\mathcal{T}}_1(\hat{\mathbf{B}}) \equiv \mathcal{T}C_{2\hat{\mathbf{B}}}$ in the $\Delta_1(\Delta_x)$-pairing, and $\tilde{\mathcal{T}}_2(\hat{\mathbf{B}}) \equiv \mathcal{T}\mathcal{M}_{\hat{\mathbf{B}}}$ in the $\Delta_2(\Delta_y)$ pairing, where $C_{2\hat{\mathbf{B}}}$ and $\mathcal{M}_{\hat{\mathbf{B}}}$ denote the twofold rotation and mirror reflection with respect to the axis $\hat{\mathbf{B}}$, respectively. These phases under in-plane Zeeman fields along appropriate directions will also be in the BDI class with Majorana flat bands on the edge. Besides, weak topological superconductivity (WTSC), the superconducting analog of weak topological insulator [42], will also be realized under appropriate in-plane Zeeman fields.

To end our discussion on topological superconductivity, we consider the specific BHZ model implemented in a square lattice with lattice constant a, anisotropic SOCs $A_{x,y}$ and in-plane Zeeman field $\mathbf{B}$

$$H_{\text{BHZ}} = A\{\tau_x\sigma_z \sin(k_y a) - \tau_y \sin(k_x a)\} + M(\mathbf{k})\tau_z + \{A_x \sin(k_x a)\sigma_y + A_y \sin(k_y a)\sigma_x\}\tau_x + \mathbf{B}\cdot\boldsymbol{\sigma}, \quad (5)$$

where $M(\mathbf{k}) = M_0 - M_1\{\cos(k_x a) + \cos(k_y a)\}$, and an in-plane Zeeman field $\mathbf{B} = (B_x, B_y, 0)$ is applied as suggested above. Near Γ point, Eq. (5) becomes Eq. (2), with $\mathcal{A} = Aa$, $\mathcal{M} = M_0 - 2M_1$, and $\mathcal{B} = M_1 a^2/2$.

We first discuss (Δ_x, Δ_y) pairing under point group D_{4h} or C_{4v}. Then the anisotropic SOCs are zero $A_{x,y} = 0$. In the chiral phase, the Chern number is proportional to the chirality and the sign of order parameter. We hence focus on $(\Delta_x, \Delta_y) = \Delta(i, 1)$ with $\Delta > 0$ in Table I, where the Chern number is essentially determined by four TRI points $\Gamma = (0, 0)$, $X = (\pi, 0)$, $(0, \pi)$ and $M = (\pi, \pi)$, whose Chern number contributions are $C_{\Gamma,M} = +2$ and $C_X = -4$. By comparing M_0, M_1 and μ, one can identify the superconducting pockets and obtain the phase diagram at zero field in Fig. 2(a). Under finite $\mathbf{B}$, every normal band splits into two spin-polarized bands, and the Chern number reads $\frac{1}{2}C(\mu - |\mathbf{B}|) + \frac{1}{2}C(\mu + |\mathbf{B}|)$, where $C(\mu)$ is the Chern number at chemical potential μ and zero field. As a result, we obtain the phase diagram under an in-plane Zeeman field in Fig. 2(b). As mentioned previously, odd Chern numbers ± 1 and -3 could arise an in-plane Zeeman field, and Majorana chiral edge states emerge correspondingly. In the nematic phase $(\Delta_x, \Delta_y) = \Delta(\cos\varphi, \sin\varphi)$, the nematic angle can be $\varphi = 0, \pi/4, \pi/2$. When $\varphi = 0(\pi/2)$, the zero-pairing lines are $\sin k_{y(x)} = 0$ or equivalently $k_{y(x)} = 0$

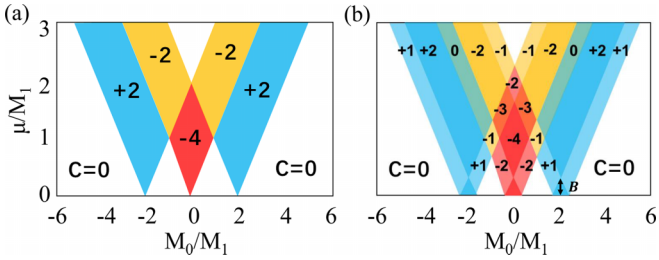

FIG. 2. Phase diagrams of chiral phase. The x axis denotes the topological parameter M_0 and the y axis denotes the chemical potential μ, both in units of M_1. (a) At zero field. (b) Under an in-plane Zeeman field $B = 0.3M_1$.

and $k_{y(x)} = \pi$, independent of applied in-plane Zeeman fields. Under an in-plane Zeeman field, as shown in Fig. 3(b), the zero-pairing lines (orange) intersect with two spin-split Fermi surface (FSs) (blue) at four nodal points labeled by their topological charges ± 1, which are all at $k_{y(x)} = 0$ line. Correspondingly, as shown in Fig. 3(e), fermionic bands (red) and Majorana flat bands (green) emerge on the open $x(y)$ edges. When $\varphi = \pi/4$, at zero field the zero-pairing lines are $\sin k_y - \sin k_x = 0$ or equivalently $k_y = k_x$ and $k_y = \pi - k_x$. Under a uniform Zeeman field, as shown in Fig. 3(c), the zero-pairing contours (orange) are not straight lines but curves depending on the Zeeman field. Such zero-pairing curves intersect with two spin-split FSs (blue contours) at four nodal points labeled by their topological charges ± 1, which are neither at $k_y = k_x$ nor $k_y = \pi - k_x$. Correspondingly, as shon in Fig. 3(f), fermionic flat bands (red) and Majorana flat bands (green) emerge on the open x edges and y vedges. In $\Delta_1(\Delta_2)$-pairing, as shown in Fig. 3(a) and 3(d), under an in-plane Zeeman field $\mathbf{B}$, the zero-pairing contours (orange) are $(\mathbf{B} \times \mathbf{k})_z = 0$ ($\mathbf{B} \cdot \mathbf{k} = 0$), which intersect with two spin-split FSs (blue contours) at four nodal points labeled by their topological charges ± 1, and Majorana flat bands (green)

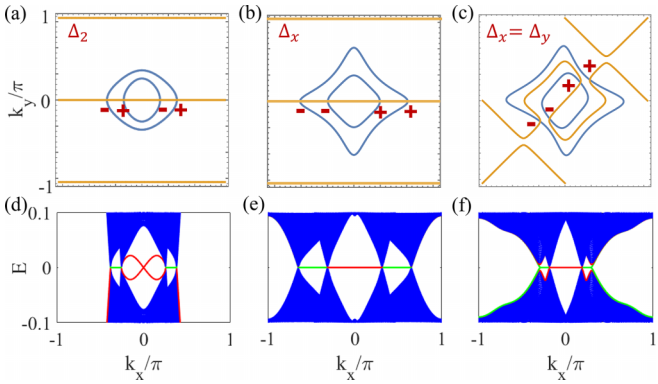

FIG. 3. Nodal superconductivity at finite field $\mathbf{B} \parallel \hat{\mathbf{x}}$. (a), (b), (c) The zero-pairing lines (orange) intersect with two spin-split Fermi surfaces (blue) at four nodal points labeled by their topological charges $\pm$. (d), (e), (f) Fermionic flat bands (red) and Majorana flat bands (green) emerge on the open x edges, corresponding to (a), (b), (c) respectively. The pairings are Δ_2 in (a), (d), Δ_x in (b), (e) and $\Delta_x = \Delta_y$ in (c), (f). Denote Δ as the pairing amplitude, the parameters are $A = M_1 = \mu = 1, A_{x,y} = 0, \Delta = 0.1$, and $(B, M_0) = (0.3, 2.5)$ in (a), (d) while $(B, M_0) = (0.1, 1.2)$ in (b), (c), (e), (f).

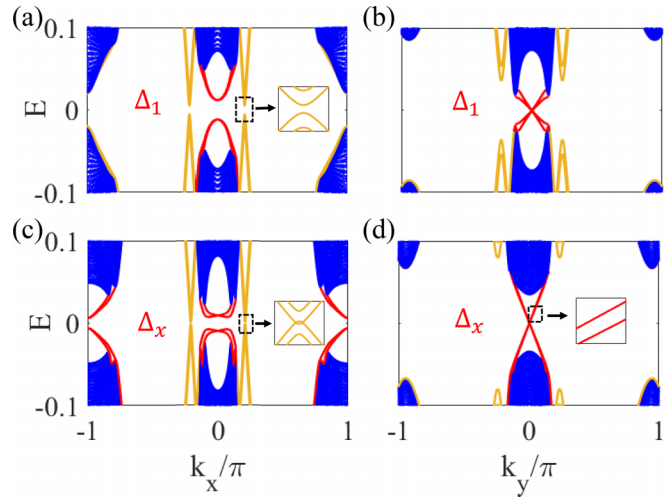

FIG. 4. Weak topological superconductivity at finite field $\mathbf{B} \parallel \hat{\mathbf{x}}$. (a), (b) Δ_1 pairing and (c), (d) Δ_x pairing. Blue regions denote bulk states, orange lines denote QSH edge states and red lines denote edge states due to pairings. The model parameters are $(A, A_x, A_y, B, M_0, M_1, \mu, \Delta, a) = (1, 0.5, 0.2, 0.05, 0.5, 1, 0.7, 0.1, 1)$ in Eq. (5).

emerge on the open edges perpendicular (parallel) to the field direction.

We then discuss $\Delta_x(\Delta_y)$ pairing under point group C_{2h}, where the anisotropic SOCs $A_{x,y}$ are finite. We define the pairing nematic direction as the $x(y)$ direction for $\Delta_x(\Delta_y)$ pairing, respectively. Under finite $\mathbf{B}$ along the twofold rotation axis (y axis in our notation), along the pairing nematic direction, Majorana flat bands can be created and QSH edge states stay unpaired, while when the Zeeman field is in the mirror plane (xz plane in our notation), WTSC will be realized along the edge perpendicular to the pairing nematic direction. As shown in Figs. 4(c) and 4(d), in Δ_x pairing, under Zeeman field $\mathbf{B} \parallel \hat{\mathbf{x}}$, QSH edge states are paired along both x and y edges, while gapless edge states exist only along y edges, which is perpendicular to the pairing nematic direction of Δ_x pairing. Our results on $\Delta_x(\Delta_y)$ pairing also apply to $\Delta_1(\Delta_2)$ pairing, respectively, as shown in Figs. 4(a) and 4(b).

So far we have considered topological superconductivity under weak in-plane fields, where the pairing potential is hardly changed by the external field. When the Zeeman field increases to the field close to the Pauli limit, the Fulde-Ferrell-Larkin-Ovchinnikov (FFLO) state [61,62] would start to emerge through a first-order phase transition, where the free energy expansion on the superconducting order parameter has to go to the sixth order as the quartic order changes sign to negative. For example, in the quartic expansion Eq. (4), under strong in-plane field larger than the Pauli limit, β could change its sign from positive to negative, triggering a first order phase transition from zero-momentum pairing phase to finite-momentum FFLO state. Finite-momentum superconductivity in the BHZ model would be discussed in our future works.

Throughout this work, we employ the mean-field theory for the analysis and calculations, which applies to regimes sufficiently away from the fluctuations. Due to the 2D nature

of the systems we consider in this manuscript, fluctuations near the superconducting transition will lead to proliferation of vortices and anti-vortices in the absence of magnetic fields, resulting in the well-known Berezinskii-Kosterlitz-Thouless transition, which would be studied in our future works.

V. CONCLUSIONS

We studied the superconducting properties of the BHZ model and proposed possible schemes for Majorana states within our framework, where in-plane Zeeman fields are always needed. As experimental candidates, we mainly discussed monolayer transition metal dichalcogenides.

ACKNOWLEDGMENTS

We thank R.-X. Zhang, H. Liu, and X. Liu for helpful discussions and important suggestions. This work is supported by the National Natural Science Foundation of China (Grant No. 12174021).

APPENDIX: EFFECTIVE PAIRINGS

We consider the full form of pairing potential

$$H_\Delta = \begin{pmatrix} 0 & \delta_1 & \delta_2 & \delta_3 \\ -\delta_1 & 0 & \delta_4 & \delta_5 \\ -\delta_2 & -\delta_4 & 0 & \delta_6 \\ -\delta_3 & -\delta_5 & -\delta_6 & 0 \end{pmatrix}, \tag{6}$$

which is an antisymmetric 4 by 4 matrix with 6 linearly independent parameters $\delta_i (i = 1, \ldots, 6)$. Another scheme of parametrization is given in the main text

$$H_\Delta = \Delta_0 i\tau_0\sigma_y + \Delta_z i\tau_z\sigma_y + \Delta_1 i\tau_y\sigma_0 + \Delta_2\tau_y\sigma_z + \Delta_x i\tau_x\sigma_y + \Delta_y\tau_y\sigma_x, \tag{7}$$

and we can find the relation between these two sets of parameters:

$$\begin{aligned} \Delta_0 &= \frac{1}{2}(\delta_2 + \delta_5), \quad \Delta_z = \frac{1}{2}(\delta_2 - \delta_5), \\ \Delta_1 &= \frac{1}{2}(\delta_1 + \delta_6), \quad \Delta_2 = \frac{i}{2}(\delta_1 - \delta_6), \\ \Delta_x &= \frac{1}{2}(\delta_3 + \delta_4), \quad \Delta_y = \frac{i}{2}(\delta_3 - \delta_4). \end{aligned} \tag{8}$$

The Cooper pairs that play the role of superconducting pairing are mainly near the Fermi energy μ (depicted in Fig. 5), and we can project the whole Hamiltonian to the states near μ and obtain the effective Hamiltonian for the paired electrons.

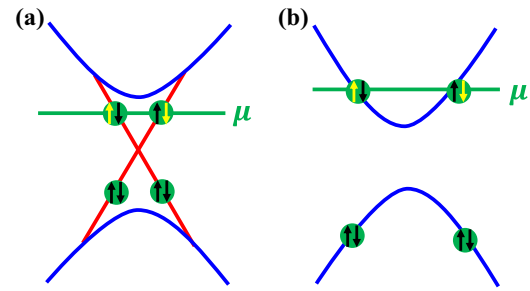

FIG. 5. Schematic of the effective pairing of bulk and edge states Project the BdG Hamiltonian of the (a) edge states, (b) bulk states into the conduction band, the yellow spin at the same Fermi energy denotes the effective pairing.

1. Effective pairing of QSH states $\Delta_{\text{edge}}(\mathbf{k})$

For the gapless edge state along $\mathbf{t} = (t_x, t_y)$ direction, the BHZ Hamiltonian Eq. (2) reduces to

$$H_{\text{edge}}(k, \mathbf{t}) = \mathcal{A}k(\sigma_z\tau_x t_y - \tau_y t_x), \tag{9}$$

where k is the edge state momentum along the edge direction and $|\mathbf{t}| = 1$ is an unit vector.

Due to time-reversal symmetry, there exists a Kramer's pair of energy-degenerate edge states with opposite momenta $k\mathbf{t}$, $-k\mathbf{t}$, and opposite spins $\uparrow, \downarrow$ at the same spatial position. However, due to the localization of edge states, the energy-degenerate edge states with opposite momenta but the same spin will be at opposite edges. As a result, equal-spin pairings are not allowed for edge states provided the on-site pairings in our work. Thus we consider the restricted form of pairing potential for the edge states

$$H'_\Delta = \begin{pmatrix} 0 & 0 & \delta_2 & \delta_3 \\ 0 & 0 & \delta_4 & \delta_5 \\ -\delta_2 & -\delta_4 & 0 & 0 \\ -\delta_3 & -\delta_5 & 0 & 0 \end{pmatrix}. \tag{10}$$

In the superconducting phase, the projected effective BdG Hamiltonian is

$$H^{\text{BdG}}_{\text{edge}}(k, \mathbf{t}) = \begin{pmatrix} \mathcal{A}k - \mu & -\Delta_{\text{edge}}(\mathbf{t})i\sigma_y \\ i\sigma_y\Delta^\dagger_{\text{edge}}(\mathbf{t}) & -\mathcal{A}k + \mu \end{pmatrix}, \tag{11}$$

where the effective pairing of QSH edge states is

$$\Delta_{\text{edge}}(\mathbf{t}) = \begin{pmatrix} \frac{1}{2}\{\delta_2 + \delta_5 - (\delta_3 + \delta_4)t_y + i(\delta_3 - \delta_4)t_x\} & 0 \\ 0 & \frac{1}{2}\{\delta_2 + \delta_5 + (\delta_3 + \delta_4)t_y - i(\delta_3 - \delta_4)t_x\} \end{pmatrix}, \tag{12}$$

For Δ_0 pairing, $\delta_2 = \delta_5 \neq 0$ and $\delta_{3,4} = 0$, thus $\Delta_{\text{edge}} = \Delta_0\sigma_0$ in this pairing channel. On the contrary for Δ_z pairing, $\delta_2 = -\delta_5 \neq 0$ and $\delta_{3,4} = 0$, thus $\Delta_{\text{edge}} = 0$ in this pairing channel. Other pairings can be similarly derived and summarized in Table I.

To be more specific, we consider the explicit examples of edge states along x and y edges in the following. Taking the ribbon geometry with the y direction opening as an example, the gapless QSH edge states emerge on the open boundary $y = 0$. Due to the translation symmetry along the

x axis, the edge states can be labeled by the momentum k_x. Due to time-reversal symmetry, there exists a Kramer's pair of energy-degenerate edge states with opposite momenta $k_x, -k_x$, and opposite spins $\uparrow, \downarrow$. The edge state Hamiltonian hence reads

$$H_{\text{edge}}(k_x) = -\mathcal{A}k_x\tau_y, \tag{13}$$

from which the edge state Kramer's pair reads

$$\phi_\uparrow = c_{1\uparrow} + ic_{2\uparrow}, \quad \phi_\downarrow = c_{1\downarrow} - ic_{2\downarrow}, \tag{14}$$

where $c_{\tau\sigma}$ denotes the electron with orbital index $\tau = 1, 2$ and spin index $\sigma = \uparrow, \downarrow$. Notice that $\phi_\uparrow$ carries momentum $+k_x$ while $\phi_\downarrow$ carries $-k_x$. Then the on-site pairing of edge states is the pairing among each Kramer's pair

$$\phi_\uparrow\phi_\downarrow = c_{1\uparrow}c_{1\downarrow} + c_{2\uparrow}c_{2\downarrow} - ic_{1\uparrow}c_{2\downarrow} + ic_{2\uparrow}c_{1\downarrow}. \tag{15}$$

The first two terms correspond to the pairing matrix Δ_0, and the last two correspond to the pairing matrix Δ_y.

For the edge states along the y axis, the Hamiltonian reads

$$H_{\text{edge}}(k_y) = \mathcal{A}k_y\sigma_z\tau_x, \tag{16}$$

and the Kramer's pair is

$$\psi_\uparrow = c_{1\uparrow} + c_{2\uparrow}, \quad \psi_\downarrow = c_{1\downarrow} + c_{2\downarrow}. \tag{17}$$

The corresponding pair matrix is

$$\psi_\uparrow\psi_\downarrow = c_{1\uparrow}c_{1\downarrow} + c_{2\uparrow}c_{2\downarrow} + c_{1\uparrow}c_{2\downarrow} + c_{2\uparrow}c_{1\downarrow}. \tag{18}$$

The first two terms correspond to the pairing matrix Δ_0, and the last two correspond to the pairing matrix Δ_x. That is, Δ_0 and Δ_x can induce gapped QSH edge states along y direction.

2. Effective pairing of bulk states $\Delta_{\text{bulk}}(\mathbf{k})$

The effective pairing of bulk states can also be obtained by the projection method. Without pairing term and magnetic field term, the BHZ Hamiltonian Eq. (5) of the manuscript can be diagonalized $U_0^{-1}(\mathbf{k})H_{\text{BHZ}}(\mathbf{k})U_0(\mathbf{k}) = \text{diag}(E, E, -E, -E)$ with eigenvalue $E = \sqrt{(A^2 + A_x^2)\sin^2 k_x + (A^2 + A_y^2)\sin^2 k_y + M^2}$ and unitary transformation $U_0(\mathbf{k})$. When adding the unconventional Δ-pairing term and magnetic field $\mathbf{B}_\parallel$, which can be regarded as perturbations, we can rewrite the whole BdG Hamiltonian on the BHZ eigenbasis $U_0(\mathbf{k})$, namely $V_0^{-1}(\mathbf{k})H_{\text{BdG}}(\mathbf{k})V_0(\mathbf{k}) = H_{\text{diag}}$ where $V_0(\mathbf{k}) = \text{diag}(U_0(\mathbf{k}), U_0^*(-\mathbf{k}))$ is the BHZ eigenbasis in the particle-hole space, and then projecting H_{diag} to conduction band, and finally obtain the effective bulk pairing in terms of conduction band electrons.

Taking Δ_1 pairing as an example, the effective bulk pairing Hamiltonian near $k_y \to 0$ is

$$(c_\uparrow, c_\downarrow)\begin{pmatrix} -\frac{i\Delta A^2 \sin k_x}{|E|} & 0 \\ 0 & -\frac{i\Delta A^2 \sin k_x}{|E|} \end{pmatrix}\begin{pmatrix} c_\uparrow \\ c_\downarrow \end{pmatrix}. \tag{19}$$

Thus, the Majorana edge states from spin up sector do not hybridize with those from the spin down sector, resulting in the gapless edge states as shown in Fig. 4(b). On the other hand, the effective bulk pairing Hamiltonian near $k_x \to 0$ is

$$(c_\uparrow, c_\downarrow)\begin{pmatrix} \frac{\Delta A^2 \sin k_y}{|E|} & -\frac{AA_y^2\Delta \sin^2 k_y}{|E|(M+|E|)} \\ \frac{\Delta(M+|E|)}{A|E|} & \frac{\Delta A^2 \sin k_y}{|E|} \end{pmatrix}\begin{pmatrix} c_\uparrow \\ c_\downarrow \end{pmatrix}. \tag{20}$$

Unlike the previous case, here the Majorana edge states from different spin sectors are coupled by the off-diagonal pairing terms in the above pairing matrix, resulting in the gapped edge states as shown in Fig. 4(a).

For Δ_x pairing, the effective bulk pairing Hamiltonian near $k_y \to 0$ is

$$(c_\uparrow, c_\downarrow)\begin{pmatrix} -\frac{i\Delta AA_x \sin k_x}{|E|} & 0 \\ 0 & \frac{i\Delta AA_x \sin k_x}{|E|} \end{pmatrix}\begin{pmatrix} c_\uparrow \\ c_\downarrow \end{pmatrix}, \tag{21}$$

which explains the gapless edge states in Fig. 4(d). The effective bulk pairing Hamiltonian near $k_x \to 0$ is

$$(c_\uparrow, c_\downarrow)\begin{pmatrix} \frac{\Delta AA_y \sin k_y}{|E|} & \frac{\Delta A^2 A_y \sin {k_y}^2}{|E|(M+|E|)} \\ \frac{\Delta(M+|E|)}{A_y|E|} & \frac{\Delta AA_y \sin k_y}{|E|} \end{pmatrix}\begin{pmatrix} c_\uparrow \\ c_\downarrow \end{pmatrix}, \tag{22}$$

which explains the gapped edge states in Fig. 4(c).

[1] M. X. Wang *et al.*, Science **336**, 52 (2012).
[2] N. Levy, T. Zhang, J. Ha, F. Sharifi, A. A. Talin, Y. Kuk, and J. A. Stroscio, Phys. Rev. Lett. **110**, 117001 (2013).
[3] S. Sasaki, M. Kriener, K. Segawa, K. Yada, Y. Tanaka, M. Sato, and Y. Ando, Phys. Rev. Lett. **107**, 217001 (2011).
[4] Z. Liu, X. Yao, J. Shao, M. Zuo, L. Pi, S. Tan, C. Zhang, and Y. Zhang, J. Am. Chem. Soc. **137**, 10512 (2015).
[5] M. P. Smylie, H. Claus, U. Welp, W. K. Kwok, Y. Qiu, Y. S. Hor, and A. Snezhko, Phys. Rev. B **94**, 180510(R) (2016).
[6] Y. Qi *et al.*, Nat. Commun. **7**, 11038 (2016).
[7] Z. Guguchia *et al.*, Nat. Commun. **8**, 1082 (2017).
[8] W. Wang, S. Kim, M. Liu, F. A. Cevallos, R. J. Cava, and N. P. Ong, Science **368**, 534 (2020).
[9] V. Fatemi, Y. Cao, L. Bretheau, Q. D. Gibson, K. Watanabe, T. Taniguchi, R. J. Cava, and P. Jarillo-Herrero, Science **362**, 926 (2018).
[10] D. A. Rhodes *et al.*, Nano Lett. **21**, 2505 (2021).
[11] E. Sajadi, T. Palomaki, Z. Fei, W. Zhao, P. Bement, C. Olsen, S. Luescher, X. Xu, J. A. Folk, and D. H. Cobden, Science **362**, 922 (2018).
[12] Z. Fei, T. Palomaki, S. Wu, W. Zhao, X. Cai, B. Sun, P. Nguyen, J. Finney, X. Xu, and D. H. Cobden, Nat. Phys. **13**, 677 (2017).
[13] S. Tang *et al.*, Nat. Phys. **13**, 683 (2017).
[14] X. Qian, J. Liu, L. Fu, and J. Li, Science **346**, 1344 (2014).
[15] F. Fei, X. Bo, R. Wang, B. Wu, J. Jiang, D. Fu, M. Gao, H. Zheng, Y. Chen, X. Wang, H. Bu, F. Song, X. Wan, B. Wang, and G. Wang, Phys. Rev. B **96**, 041201(R) (2017).
[16] C. Liu, C.-S. Lian, M.-H. Liao, Y. Wang, Y. Zhong, C. Ding, W. Li, C.-L. Song, K. He, X.-C. Ma, W. Duan, D. Zhang, Y. Xu, L. Wang, and Q.-K. Xue, Phys. Rev. Mater. **2**, 094001 (2018).

[17] H. Leng, J. C. Orain, A. Amato, Y. K. Huang, and A. de Visser, Phys. Rev. B **100**, 224501 (2019).
[18] Y. Yuan, J. Pan, X. Wang, Y. Fang, C. Song, L. Wang, K. He, X. Ma, H. Zhang, F. Huang, W. Li, and Q.-K. Xue, Nat. Phys. **15**, 1046 (2019).
[19] Y. Fang *et al.*, Adv. Mater. **31**, 1901942 (2019).
[20] Y. W. Li *et al.*, Nat. Commun. **12**, 2874 (2021).
[21] S. Cho *et al.*, Nano Lett. **22**, 8827 (2022).
[22] E. Zhang *et al.*, Nat. Phys. **19**, 106 (2023).
[23] S. Kezilebieke, M. N. Huda, V. Vaňo, M. Aapro, S. C. Ganguli, O. J. Silveira, S. Głodzik, A. S. Foster, T. Ojanen, and P. Liljeroth, Nature (London) **588**, 424 (2020).
[24] Di Xiao, G.-B. Liu, W. Feng, X. Xu, and W. Yao, Phys. Rev. Lett. **108**, 193904 (2012).
[25] N. F. Q. Yuan, K. F. Mak, and K. T. Law, Phys. Rev. Lett. **113**, 097001 (2014).
[26] A. Ribak, R. M. Skiff, M. Mograbi, P. K. Rout, M. H. Fischer, J. Ruhman, K. Chashka, Y. Dagan, and A. Kanigel, Sci. Adv. **6**, eaax9480 (2020).
[27] A. K. Nayak, A. Steinbok, Y. Roet, J. Koo, G. Margalit, I. Feldman, A. Almoalem, A. Kanigel, G. A. Fiete, B. Yan, Y. Oreg, N. Avraham, and H. Beidenkopf, Nat. Phys. **17**, 1413 (2021).
[28] X. Wu, S. Qin, Y. Liang, H. Fan, and J. Hu, Phys. Rev. B **93**, 115129 (2016).
[29] Z. F. Wang, H. Zhang, D. Liu, C. Liu, C. Tang, C. Song, Y. Zhong, J. Peng, F. Li, C. Nie, L. Wang, X. J. Zhou, X. Ma, Q. K. Xue, and F. Liu Nat. Mater. **15**, 968 (2016).
[30] X. Shi, Z.-Q. Han, P. Richard, X.-X. Wu, X.-L. Peng, T. Qian, S.-C. Wang, J.-P. Hu, Y.-J. Sun, and H. Ding, Sci. Bull. **62**, 503 (2017).
[31] D. Wang, L. Kong, P. Fan, H. Chen, S. Zhu, W. Liu, L. Cao, Y. Sun, S. Du, J. Schneeloch, R. Zhong, G. Gu, L. Fu, H. Ding, and H.-J. Gao, Science **362**, 333 (2018).
[32] Q. Liu, C. Chen, T. Zhang, R. Peng, Y. J. Yan, Chen-Hao-Ping Wen, X. Lou, Y. L. Huang, J. P. Tian, X. L. Dong *et al.*, Phys. Rev. X **8**, 041056 (2018).
[33] P. Zhang, K. Yaji, T. Hashimoto, Y. Ota, T. Kondo, K. Okazaki, Z. Wang, J. Wen, G. D. Gu, H. Ding, and S. Shin, Science **360**, 182 (2018).
[34] P. Zhang *et al.*, Nat. Phys. **15**, 41 (2019).
[35] X. L. Peng, Y. Li, X.-X. Wu, H.-B. Deng, X. Shi, W.-H. Fan, M. Li, Y.-B. Huang, T. Qian, P. Richard, J.-P. Hu, S.-H. Pan, H.-Q. Mao, Y.-J. Sun, and H. Ding, Phys. Rev. B **100**, 155134 (2019).
[36] W. Liu, L. Cao, S. Zhu, L. Kong, G. Wang, M. Papaj, P. Zhang, Y.-B. Liu, H. Chen, G. Li, F. Yang, T. Kondo, S. Du, G.-H. Cao, S. Shin, L. Fu, Z. Yin, H.-J. Gao, and H. Ding, Nat. Commun. **11**, 5688 (2020).
[37] C. Chen, K. Jiang, Y. Zhang, C. Liu, Y. Liu, Z. Wang, and J. Wang, Nat. Phys. **16**, 536 (2020).
[38] N. Read and D. Green, Phys. Rev. B **61**, 10267 (2000).
[39] A. Y. Kitaev, Phys. Usp. **44**, 131 (2001).
[40] D. A. Ivanov, Phys. Rev. Lett. **86**, 268 (2001).
[41] L. Fu and C. L. Kane, Phys. Rev. Lett. **100**, 096407 (2008).
[42] X. L. Qi and S. C. Zhang, Rev. Mod. Phys. **83**, 1057 (2011).
[43] C. Nayak, S. H. Simon, A. Stern, M. Freedman, and S. Das Sarma, Rev. Mod. Phys. **80**, 1083 (2008).
[44] J. Alicea, Y. Oreg, G. Refael, F. V. Oppen, and M. P. A. Fisher, Nat. Phys. **7**, 412 (2011).
[45] X. J. Liu, C. L. M. Wong, and K. T. Law, Phys. Rev. X **4**, 021018 (2014).
[46] G. Xu, B. Lian, P. Tang, X. L. Qi, and S. C. Zhang, Phys. Rev. Lett. **117**, 047001 (2016).
[47] X. L. Qi, T. L. Hughes, and S. C. Zhang, Phys. Rev. B **82**, 184516 (2010).
[48] C.-Z. Chang *et al.*, Science **340**, 167 (2013).
[49] J. Wang, Y. Xu, and S.-C. Zhang, Phys. Rev. B **90**, 054503 (2014).
[50] C. L. Kane and E. J. Mele, Phys. Rev. Lett. **95**, 226801 (2005).
[51] B. A. Bernevig, T. L. Hughes, and S. C. Zhang, Science **314**, 1757 (2006).
[52] M. König, S. Wiedmann, C. Brüne, A. Roth, H. Buhmann, L. W. Molenkamp, X.-L. Qi, and S.-C. Zhang, Science **318**, 766 (2007).
[53] R. X. Zhang, W. S. Cole, X. Wu, and S. Das Sarma, Phys. Rev. Lett. **123**, 167001 (2019).
[54] R. X. Zhang and S. Das Sarma, Phys. Rev. Lett. **126**, 137001 (2021).
[55] X. Wu, X. Liu, R. Thomale, and C. X. Liu, Natl. Sci. Rev. **9**, nwab087 (2022).
[56] S. Qin, C. Fang, F. C. Zhang, and J. Hu, Phys. Rev. X **12**, 011030 (2022).
[57] A. P. Schnyder, S. Ryu, A. Furusaki, and A. W. W. Ludwig, Phys. Rev. B **78**, 195125 (2008).
[58] J. C. Y. Teo and C. L. Kane, Phys. Rev. B **82**, 115120 (2010).
[59] M. Sato, Y. Tanaka, K. Yada, and T. Yokoyama, Phys. Rev. B **83**, 224511 (2011).
[60] N. F. Q. Yuan, C. L. M. Wong, and K. T. Law, Physica E **55**, 30 (2014).
[61] P. Fulde and R. A. Ferrell, Phys. Rev. **135**, A550 (1964).
[62] A. I. Larkin and Y. N. Ovchinnikov, Sov. Phys. JETP **47**, 1136 (1964).